ASTRONOMY & ASTROPHYSICS
SUPPLEMENT SERIES

APRIL II **1997**, PAGE 357

Astron. Astrophys. Suppl. Ser. **122,** 357-369 (1997)

The high energy instrument PDS on-board the BeppoSAX X–ray astronomy satellite

F. Frontera[1,2], E. Costa[3], D. Dal Fiume[1], M. Feroci[3], L. Nicastro[1], M. Orlandini[1], E. Palazzi[1], and G. Zavattini[2]

[1] Istituto Tecnologie e Studio Radiazioni Extraterrestri, CNR, Via Gobetti, 101, 40129 Bologna, Italy
[2] Dipartimento di Fisica, Università di Ferrara, Via Paradiso, 11, 44100 Ferrara, Italy
[3] Istituto di Astrofisica Spaziale, CNR, Via E. Fermi, 21, 00044 Frascati, Italy

Received May 15; accepted June 3, 1996

Abstract. BeppoSAX/PDS experiment is one of four narrow field instruments of the BeppoSAX payload, that also includes two wide field cameras. The goal of PDS is to extend the energy range of BeppoSAX to hard X–rays. The operative energy range of PDS is 15 to 300 keV, where the experiment can perform sensitive spectral and temporal studies of celestial sources. The PDS detector is composed of 4 actively shielded NaI(Tl)/CsI(Na) phoswich scintillators with a total geometric area of 795 cm^2 and a field of view of 1°.3 (FWHM). In this paper we describe the experiment design and discuss its functional performance and calibration data analysis system.

Key words: instrumentation: detectors — space vehicles — X–ray: general

1. Introduction

The BeppoSAX satellite is a joint program of the Italian Space Agency (ASI) and the Netherlands Agency for Aerospace Programs (NIVR) devoted to X–ray astronomical observations in a broad energy band ($0.1 - 300$ keV). BeppoSAX is scheduled to be launched in April 1996 into a circular orbit at 600 km altitude with an inclination of about 3°. The above inclination was chosen to get a high geomagnetic cut-off with a very low modulation and to minimize the induced radiation on the payload due to the South Atlantic Anomaly (SAA). Overviews of the BeppoSAX mission can be found elsewhere (Butler & Scarsi 1990; Scarsi 1993; Piro et al. 1995). The satellite is three–axis–stabilized with post-facto attitude reconstruction with 1 arcmin accuracy. Its expected lifetime is from 2 years up to 4 years. The payload includes Narrow Field Instruments (NFI) and Wide Field Cameras (WFC). The NFIs are four Concentrators Spectrometers (C/S) with 3 units (MECS) operating in the $1 - 10$ keV energy band and 1 unit (LECS) operating in $0.1 - 10$ keV, a High Pressure Gas Scintillation Proportional Counter (HPGSPC) operating in the $3 - 120$ keV energy band and a Phoswich Detection System (PDS) with four detection units operating in the $15 - 300$ keV energy band. Orthogonally with respect to the NFIs there are two WFCs (field of view of $20° \times 20°$ FWHM) which operate in the $2 - 30$ keV energy band with imaging capabilities (angular resolution of 5 arcmin). As a part of the PDS, there is a Gamma Ray Burst Monitor (GRBM) with nominal energy band of 60 to 600 keV.

As can be seen, BeppoSAX covers an unprecedented wide energy band from 0.1 to 300 keV. The hard X–ray energy band ($15 - 300$ keV) covered by the PDS experiment is now assuming key importance for high energy astrophysics thanks to many exciting and unexpected results obtained with γ-ray astronomy experiments like BATSE and OSSE aboard CGRO, SIGMA aboard the GRANAT satellite and balloon experiments. In addition to well known classes of strong hard X–ray emitters (galactic X–ray pulsars, black hole candidates, Am Her-type sources, AGN), other classes of X–ray sources, like X–ray bursters, resulted to be strong hard X–ray emitters during source states when the low energy emission is relatively weak (Barret & Vedrenne 1994; Zhang et al. 1996). These sources were not expected to have hard emission spectra. Soft gamma ray repeaters have been discovered. Some of them exhibit parossistic phases of activity, during which up to ~ 40 bursts per day are detected (Kouveliotou et al. 1996; Lewin et al. 1996). Also for extragalactic sources the hard X–ray sky was full of unexpected results, e.g. for Seyfert 2 (Bassani et al. 1996).

With its high sensitivity, especially in the $20 - 100$ keV band, PDS will offer the opportunity to perform observations of key importance in the hard X–ray band. Many open questions in high energy astrophysics are expected

Send offprint requests to: frontera@tesre.bo.cnr.it

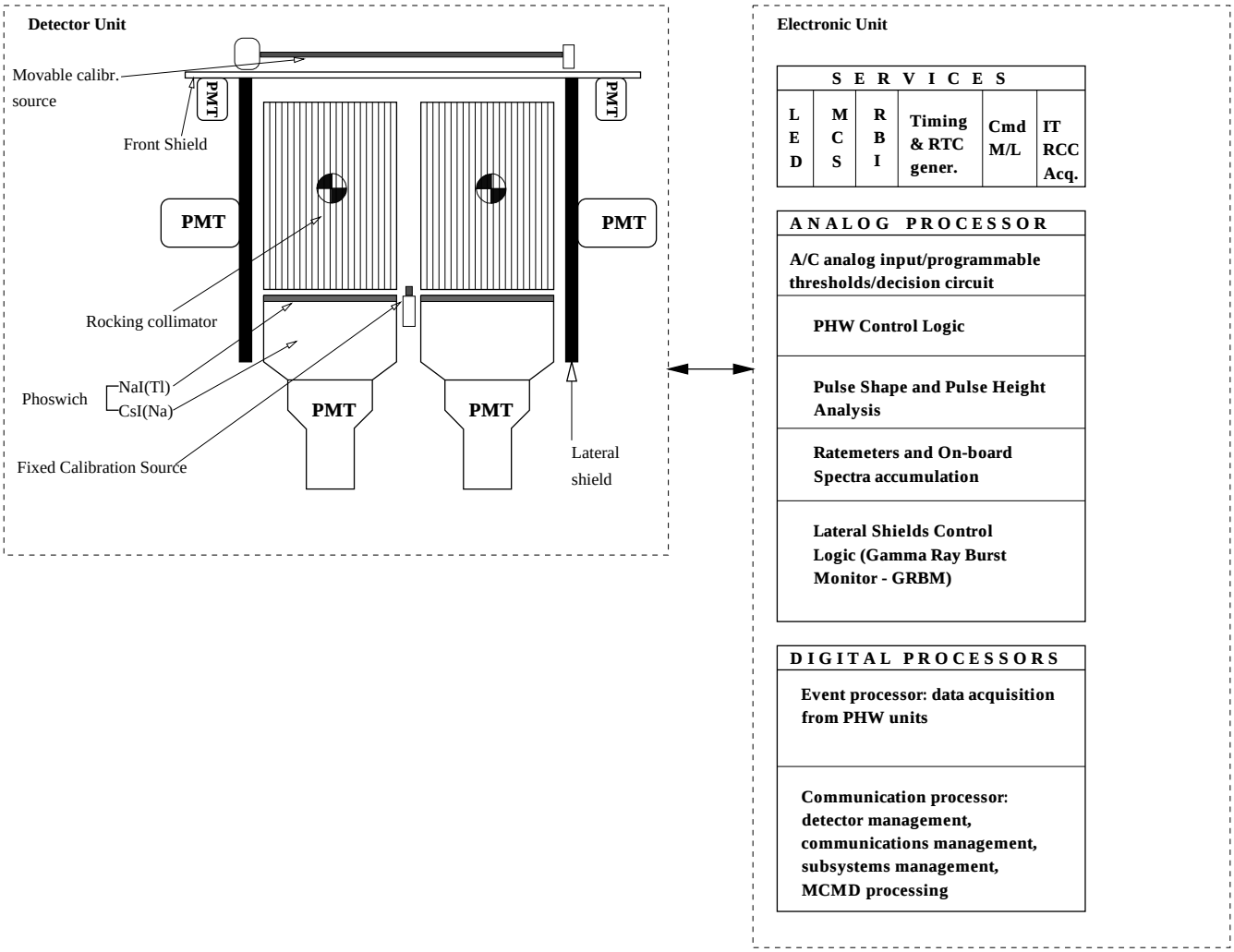

Fig. 1. A sketch of the major components of the PDS experiment

to be clarified and solved with observations in this band. Coordinated observations with GRO–BATSE and XTE will give the opportunity to fully exploit the joint capabilities of the three observatories that cover this important energy band. Also coordinated observations with on-ground and space observatories are extremely important for identifying counterpart of new hard X–ray sources and/or study the complex physics occurring in them.

In this paper we will give a description of the PDS and of its performances as derived from functional tests and pre-flight calibrations. Descriptions of the PDS design have already been reported (Frontera et al. 1991, 1992). Also reported are preliminary results obtained from instrument functional tests (Frontera et al. 1997). The GRBM expected performance has also been investigated and results were reported (Pamini et al. 1990; Alberghini et al. 1994).

2. Instrument description

A sketch of the major components of the PDS experiment is shown in Fig. 1, and a summary of its main features is given in Table 1.

The PDS consists of a square array of four independent NaI(Tl)/CsI(Na) scintillation detectors. A system of anticoincidence (AC) shields surrounds the sides and the front of the detectors and collimators, that limit the telescope field of view (FOV). There are two independent collimators, one for each pair of detectors. Each collimator bench can be independently rocked back and forth to allow the simultaneous monitoring of source and background. The gain of the detectors and of the associated electronic chain is continuously monitored and automatically controlled by using as sensor a fixed calibration source (FCS) of Am^{241}. The instrument can also be periodically in-flight calibrated with a movable calibration source (MCS). The AC lateral shields are also used as gamma-ray burst monitor. Finally a particle monitor (PM) provides information

Table 1. Main features of the PDS experiment

PARAMETER	VALUE
Energy range	$15 - 300$ keV
NaI(Tl) phoswich thickness	3 mm
CsI(Na) phoswich thickness	50 mm
Total area through collimator	640 cm^2
Field of view (FWHM)	1.3° hexagonal
Energy resolution at 60 keV	$\leq 15\%$ (on the average)
Maximum time resolution	16 μs
Gain control accuracy	0.25%
In-flight calibration accuracy	0.1%
Minimum channel width of energy spectra	0.3 keV
Maximum throughput	4000 events s^{-1}

on high environmental particle fluxes and triggers actions to prevent the damage of the detectors photomultipliers (PMT). All events detected in the PDS detector are processed by an Analog Processor (AP), that includes all the analog electronics, analog-to-digital converters (ADCs), AC logics, programmable thresholds. Each detected event qualified as a good one by the AP is time tagged and sent to a Digital Processor (DP) for the data processing via a 40 bit FIFO. The DP filters and formats the data that are finally sent via Block Transfer Bus to the BeppoSAX On-Board Data Handling (OBDH). The AP and DP constitute the PDS Instrument Controller (IC).

In the following subsections the main elements of PDS are described.

2.1. Detection plane

The detection plane of PDS is an array of four scintillation detectors. Each of the four detectors is composed by two crystals of NaI(Tl) and CsI(Na) optically coupled and forming what is known as **PHOSWICH** (acronym of PHOsphor sandWICH). The NaI(Tl) thickness is 3 mm and the CsI(Na) thickness is 50 mm.

The scintillation light produced in each phoswich (PHW) is viewed, through a quartz light guide, by a PMT EMI D-611. The NaI(Tl) acts as the X–ray detector, while the CsI(Na) scintillator acts as an active shield. The scintillation events (due to photons or charged particles) detected by each phoswich can be divided into three classes: those that deposit energy only in the NaI crystal (NaI events or "good events"); those that deposit energy only in the CsI crystal (CsI events); those that deposit energy in both crystals (mixed events). The events of the first class are accepted, while the events of the other two classes are rejected. The rejection is performed using the different decay constants of the scintillations produced in the NaI (about 0.25 μs at room temperature) and CsI (0.6 μs and about 7μs for CsI). The analysis electronics (see Sect. 2.7), via its Pulse Shape Analyzer (PSA), is capable to discriminate events of the classes described above. Figure 2 shows a typical pulse shape spectrum in the $15 - 300$ keV range. It is characterized by two peaks, one (on the left) due to NaI(Tl) events and the other due to CsI(Na) events. The scale in abscissa is correlated with the decay time of the scintillation pulses.

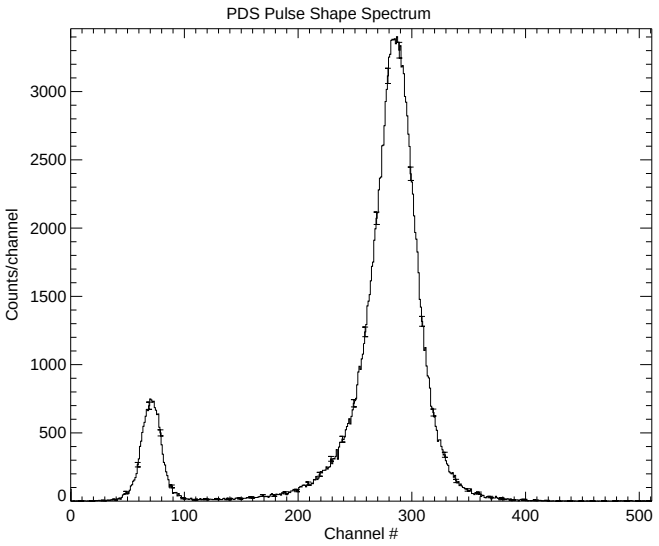

Fig. 2. Typical pulse shape spectrum in the $15 - 300$ keV energy range. Note the discrimination between NaI "good" events (left) and CsI events (right)

The selection of good events is performed through the choice of lower and upper programmable PSA thresholds in the Electronic Unit (see below).

The phoswich configuration is well known to provide a high detection efficiency and a very low background level. In addition, taking into account that the accepted photons lose energy in the NaI(Tl) alone, the energy spectra provided by phoswiches are not affected by biases as in single crystal detectors. The total geometric detection area is 795 cm^2. The other crystal parameters are given in Table 1.

2.2. Collimator assembly

The collimator assembly consists of two X–ray collimators made of Tantalum tubes with hexagonal section. Inside each tube, a 4 cm bi-layer of Tin plus Copper is inserted. The role of Tin, 100 μm thick, is to attenuate K-fluorescence emission from the Tantalum (K_α = 57.07 keV, K_β = 65.56 keV), while the Copper, 50 μm thick, was used to attenuate the K-fluorescence emission from Tin (K_α = 25.1 keV, K_β = 28.5 keV). This cell configuration is known as graded shielding. The detector net area through collimators is 80% of the total geometric area.

The collimators limit the detector field of view to 1°.3 Full Width at Half Maximum (FWHM). Each of the two collimators can be independently rocked back and forth with respect to the neutral position directed along the detector axis. Five symmetrical rocking steps are provided on each side of the neutral position. The maximum rocking angle is ± 210′ (3.5 degrees) and the intermediate steps are ± 30′, ± 60′, ± 90′, ± 150′.

The standard observation strategy is to continuously monitor background and source+background with both collimators using a cyclic law: while one of the two collimators points to the source the other one points to a blank (non source-contaminated) sky field for background measurement. At each cycle the two collimators are swapped: the one pointing to the source is moved to monitor background and viceversa. The default collimator law samples alternatively two background fields on the two opposite sides of the observed source at the maximum rocking angle. Therefore the default full cycle is ON /+210′(OFF) / ON /−210′ (OFF). As the collimator law is fully programmable, any other convenient choice can be made. As an example, if one of the two background fields is contaminated by the presence of an unwanted source, a suitable law that rocks the collimators only on one side, or that changes the rocking angle to a value which excludes contamination, can be chosen. It is also possible to move the collimators through all the allowed positions. In this way one can derive the angular response of the collimators to a given source and the source position can be determined.

The dwell time (minimum 50 s) in each collimator position can be chosen from ground.

A position transducer gives an independent high accuracy (about 1 arcsec) monitoring of the collimator position for each collimator. This monitoring is transmitted to ground in the housekeeping (HK) data stream with a sampling rate of 1 s.

2.3. Detector window

The X–rays entering through the telescope FOV cross the top shield materials and the entrance window of the phoswich crystals (kept under vacuum). The top shield window is made of 1000 μm BC-434 plastic scintillator covered with aluminized Kapton (0.8 μm Al plus 200 μm Kapton). The phoswich window is made of 1500 μm Be, 890 μm Silicone rubber, aluminized Kapton (0.1 μm Al plus 76 μm Kapton) and 100 μm Teflon film. The Silicone rubber was used to provide thermal and mechanical insulation, the Teflon film was used as light reflective material, while the aluminized Kapton was used as a barrier between the Silicone rubber and the reflective material.

2.4. Anticoincidence shield system

A further reduction in the intrinsic background of PDS is achieved using a five sides anticoincidence shield system. This consists of the lateral and top shield assemblies, both highly efficient in the rejection of events due to charged particles. The CsI(Na) lateral shields are also very efficient as active shields of photons coming from the sides.

In the following we describe this subsystem and the anticoincidence logics used to operate it.

2.4.1. Lateral shield assembly

The lateral shielding system is made of four optically independent slabs of CsI(Na) scintillators 10 mm thick, 275 mm high and 402 mm wide. Each slab is made of two pieces optically coupled together. Each slab is viewed, through a quartz light pipe, by two 3″ PMTs (Hamamatsu R-2238) with independent high voltage power supplies. In order to monitor the gain of each detector, a light pulser made of an Am^{241} source encapsulated in a small NaI(Tl) scintillator is inserted into each slab to produce pulses equivalent to photons with energy within the range from 350 to 450 keV, depending on the particular scintillator slab. The summed signals from each slab are sent to a programmable threshold for the AC logic. If the summed signal is above the AC threshold, a veto signal is generated by the PDS analog processor.

2.4.2. Top shield assembly

The top shield assembly consists of a 1 mm thick plastic scintillator (BC-434) viewed by four PMTs (Hamamatsu R-1840) with independent power supplies. It is located above the collimator assembly and covers the entire telescope FOV. This shield was included in the PDS design to reject the background events due to charged particles entering the aperture of the instrument that deposit part of their energy in the top shield. In particular we expect that this shield is effective in rejecting events generated by high energy electrons. These electrons are expected to be produced by interactions of Cosmic Rays with the satellite materials.

The summed signal from the four PMTs is sent to a programmable analog threshold for the AC logic. If the summed signal is above the AC threshold, a veto signal is generated by the PDS analog processor.

2.4.3. Anticoincidence shield with other PHW units

Any event that is detected from one of the four PHW units is compared with a programmable analog AC threshold. If the signal is above this threshold, a logic signal is set. A veto signal is generated by the PDS analog processor if at least two units set this logic signal. This happens when two or more simultaneous events are detected from the PHW units above their A/C thresholds. In this way we reject events that interact with one of the NaI scintillators via Compton effect, leaving only a fraction of their energy in it, while the photon with the remaining energy is absorbed in other PHW unit(s).

2.4.4. AC logic and operative modes

The AC system acts as a logical OR among the AC veto signals issued by the PDS Analog Processor. The decision time of the AC logic is programmable with 5 equispaced steps between 2 and 10 μs independently for each of the AC signals described in the previous sections. The AC logics are permanently activated with two operative modes selectable from the ground: AC–ON in which the vetoed events are not transmitted to ground; AC–OFF, in which the vetoed events are flagged and transmitted to ground. This last mode can be used only when PDS is transmitting data in some Direct Modes (see Sect. 2.7). The AC of each PHW unit, of the lateral shields and of the front shields can be separately programmed to be ON or OFF.

2.5. Automatic gain control

The automatic gain control of the phoswich detectors (AGC) is implemented as follows. At the center of the detection plane there is a fixed calibration source (FCS). It consists of an Am^{241} radioactive source distributed within a plastic scintillator (BC-400) viewed by a PMT (Hamamatsu R 1635). Part of the 60 keV X–rays emitted by this source impinges on the four phoswich detectors. These events are tagged thanks to the 5.5 MeV α particles simultaneously emitted with them and detected by the plastic scintillator.

The rate of 60 keV photons detected by each phoswich as pure NaI events ranges from 3.6 to 4.4 s^{-1} depending on the phoswich unit.

The signal from the PMT coupled to the plastic scintillator is used by the PDS electronics to tag the photons simultaneously detected by the PHWs. The tagging efficiency is about 98%. The tagged photons are used by the PDS IC to detect gain variations and to perform a continuous and automatic gain correction by acting on the high voltage supplies of the phoswich PMTs. This correction is operated using two prefixed contiguous channel windows, with the separation channel corresponding to the Am^{241} 60 keV peak position at nominal gain. Each time a NaI event tagged as Am^{241} event is inside the left window or the right window, the HV of the corresponding phoswich is changed by +97 mV or −97 mV, respectively. The spectra of the tagged Am^{241} photons are transmitted with the housekeeping information with 128 s integration time.

The AGC is operated by the PDS DP. It is therefore completely reprogrammable from ground, if needed.

The FCS is not suitable to be used as an absolute calibrator, since the FCS photons impinge only on a small part of the phoswich detector surfaces, close to the centre of the detection plane. Due to disuniformity in the scintillation light collection across the crystal surface, a bias in the detector gain should derive. Absolute gain measurement can be performed using the in–flight calibration system described in the next section.

2.6. In-flight calibration

The in-flight calibration of the PDS is performed by means of two different devices: a Movable Calibration System (MCS) and a light pulser.

2.6.1. Movable calibration system

The movable calibrator MCS is made of a radioactive source of Co^{57} (main lines at 14.37, 122.06 and 136.47 keV) distributed along a wire of about 32 cm length, and contained in a cylinder of lead that shields the radioactive source but a small aperture directed toward the crystal assembly. The MCS, upon an on-ground command, performs a scan of the entire field of view of the instrument above the collimators and top shield at constant speed, uniformly irradiating all the PHWs. Given the limited half life of the source (271 days), the calibrator crossing speed can be varied in order to get the needed statistical quality of the source data.

2.6.2. Light pulser

A light pulser (LED) is encapsulated in each phoswich crystal. It allows to simulate a prefixed gamma equivalent energy (GEE) lost in the phoswich. In this way the gain of the phoswich PMTs and electronic chain can be checked. The LED is mainly used for diagnostic purposes.

2.7. Electronic unit

The electronic unit includes a power supply module and, as discussed above (see Sect. 2), the AP, which is devoted to analog data processing and digital conversion, and DP. This has in charge two tasks: the PDS data management and the instrument control. The DP includes two microprocessors (type 80 C86): one (the Event Processor, EP) to perform the first task and the other (the Communication Processor, CP) to perform the second task. Both processors make use of hybrid circuits.

The pulses from each phoswich unit with amplitude in the band corresponding to the operative energy band of PDS that pass the AC logic are pulse height and pulse shape analyzed.

The AC logic allows to reject one or more of the following types of events detected by the phoswich units:

1. Events simultaneous with events above the AC threshold of the lateral shields;
2. Events simultaneous with events above the AC threshold of the top shield;
3. Events simultaneous with events detected by other phoswich units with energy above their AC threshold.

If one or more of the above coincided events are accepted, they can be transmitted with the proper AC flag in case of Direct Transmission Mode. By default the AC logic rejects all the event types from 1 to 3 or any combination of them.

The pulse shape analysis is performed using a constant fraction/crossover PSA. For a detailed description of the PSA and of its performance see Frontera et al. (1993).

The pulse height analysis is performed by a 12 bit successive approximation analog-to-digital converter (ADC) with the sliding scale technique. This technique was chosen to improve the average differential linearity of the pulse height channels. The ADC conversion time is 5 μs.

The selection of the good events, corresponding to energy losses only in the NaI(Tl) scintillator, is performed through the setting of lower and upper pulse shape digital thresholds. These thresholds are operated by the EP.

The qualified events are formatted by the EP in different transmission modes before being acquired by the On-Board Data Handling (OBDH). The transmission modes can be direct and indirect. Direct Modes (DM) transmit information about each qualified event detected by PDS. The information that can be transmitted to ground is:

- energy: maximum 10 bits
- pulse shape: maximum 9 bits
- event time: maximum 16 bits
- unit identity: 2 bits
- AC flags: 3 bits (one for each AC type).

This maximum information can be compressed in two ways: by masking some bits (the less significant bits) of each field or by eliminating one or more fields. Fourteen predefined compressions are available on board: the maximum event size is 5 bytes (40 bits); the minimum event size is 2 bytes (16 bits).

In Indirect Spectral Mode, the qualified events are accumulated in energy spectra histograms, one for each detection unit. For these integrated spectra the number of energy channels (128 or 256), the maximum content of each channel (8 or 16 bits), and the accumulation time (5 choices, between 1 and 32 s) can be independently set. The indirect spectral modes can be run in parallel with temporal modes. These modes allow the transmission of histograms with count rate time profiles in 1 to 4 energy bands with time resolution down to 1 ms.

In addition to the information associated with good events, other housekeeping (HK) information is provided by the DP and transmitted. This includes pulse shape spectra of the phoswich units in the entire energy band, energy spectra of the FCS, various ratemeters, dead time counters, status information and technological data (high voltage and low voltage checks, temperature of different instrument components, status of the MCS and collimator motors). The HK spectra are summed on time intervals of 128 s, the ratemeters are integrated over 1 s, while the technological data are sampled and transmitted with variable rate, from 16 to 64 s depending on the data type.

2.8. Gamma-ray burst monitor

The lateral shields of the PDS are also used as detectors of gamma-ray bursts of cosmic origin (GRB). The signals from each of the slabs in a programmable energy band, nominally $60 - 600$ keV (the low threshold can be lowered down to about 20 keV), are sent to both a Pulse Height Analyser and a GRBM logic unit, where the trigger condition is checked. A GRB event is triggered when at least two of the four lateral shields meet the trigger condition. In this way we expect to reduce the rate of false triggers caused by interactions of high energy particles in the shields. If a GRB condition is verified, the burst time profiles in the entire energy band from each of the four detectors are stored, together with the absolute time of the trigger occurrence. The integration time for count accumulation will be 7.8 ms for 10 s preceeding the trigger, 0.48 ms for 10 s immediately following the trigger and 7.8 ms from 10 s to about 2 minutes after the trigger time. Along with burst profiles, energy spectra integrated over 128 s and ratemeters integrated over 1 s in the GRBM energy thresholds are continuously acquired.

Parameters of the trigger logic are programmable from the ground. Details on GRBM and its performance will be published in a separate paper in preparation.

2.9. Particle Monitor (PM)

A particle detector, made of BC-434 plastic scintillator viewed by a PMT (R-1840), is mounted close to the PDS instrument position in the satellite. The detector has a cylindric-like shape with a diameter of 2 cm and a thickness of 5 mm. It is covered on the top and sides with an aluminum frame of 2 mm thickness. This configuration provides an energy threshold that for electrons is about 1.2 MeV and for protons is 20 MeV. The PM is used to switch off the high voltage supplies of all the PMTs, excluding the PM PMT itself, when the environmental charged particle count rate integrated over 32 s will exceed a programmable threshold and to switch them on again when this level is below another programmable threshold.

3. Instrument performance

The instrument performance was derived by means of various tests performed at different levels. Functional tests on the most critical items were performed at component level (phoswich units, FCS, shield assembly, collimators, PSA). Preliminary results of the functional tests have already been reported (Frontera et al. 1997).

The instrument calibration was performed in successive steps. First the Core Assembly (detection plane plus FCS) was separately calibrated from the Shield Assembly (top shield plus lateral shield plus MCS) and rocking collimators. The rocking collimators were not integrated in the detector in order to irradiate each phoswich detection unit with almost uniform X–ray beams obtained with radioactive sources at a distance of 1.8 m (see Sect. 3.2).

Then the core assembly was integrated with the shield assembly with MCS source not mounted. A new

calibration of the detection plane was then performed and compared with the previous one. Comparing the line intensities measured with this calibration with the corresponding ones measured before, we were capable to get an experimental verification of the expected X–ray transparency of the top shield.

Then the rocking collimators were integrated with the detector. In this configuration the CsI(Na) slabs of the lateral shields and the plastic scintillator of the top shield were calibrated. Also the AC thresholds, the AC decision time, the pulse height thresholds, the rise time thresholds for selecting NaI events were calibrated and set. The background level was also accurately measured. Finally the MCS source was mounted in its frame and more calibrations were performed and compared with the previous ones. The detector contamination by MCS source, its background behaviour as a function of the collimator rocking angle and MCS count rate as a function of the collimator offset were investigated.

AGC performance was investigated during the first calibration campaign. After that, it was continuously used during the subsequent calibration tests.

During all the calibration tests, the flight electronic unit was used. Events from the phoswich units were all acquired in direct mode, with the maximum information associated to each event (see Sect. 2.7). In addition all the other available HK information were acquired. The encoded data from the experiment were sent to a simulator of the BeppoSAX OBDH and then to a mass memory. In parallel, the encoded data from the OBDH simulator were acquired by a PDS dedicated computer system (Dal Fiume et al. 1994, 1995) for an on-line filing of the data, quick look display, scientific analysis and archiving.

3.1. Monte Carlo tool

In order to derive the response function of the PDS instrument, in addition to the calibration tests, a Monte Carlo code based on EGS4 (Nelson et al. 1985) was developed. The geometry described in the simulation of the detector included the top shield assembly, the four phoswich units including the quartz light guides, and the entrance window composition and the four Lateral Shields. The X–ray interactions simulated by EGS4 code include photoelectric absorption, Compton scattering, K-fluorescence production and transport. All photons were followed down to 5 keV. The transport of the electrons produced in the photon interactions was also included down to a minimum energy of 10 keV. Finally the electronic analysis of the light pulses was calculated to reproduce the pulse-shape analysis and energy spectra. The pulse-shape distribution was reproduced assuming a Poisson statistics of the light decay-time of the scintillators and calculating the variance and covariance of the electronic outputs. For the energy spectra the measured calibration and resolution was used. We assumed for the NaI(Tl) scintillation an exponential time distribution with decay constant of 0.23 μs, while for the CsI(Na) we assumed the weighted sum of two exponential functions with decay constants of 0.65 μs and 7 μs, respectively (Bleeker & Overtoom 1979). These values are suitable to describe the scintillations at room temperature.

In this way we can compare the calibration spectra measured with the expected ones as will be discussed in Sect. 3.3.3.

3.2. Radioactive sources for experiment calibration

The radioactive sources used for the experiment calibration included Am^{241}, Cd^{109}, Co^{57}, Ce^{139} and Hg^{203}, Na^{22}, Sn^{113} and Cs^{137}. They were contained in proper wells of Lead that acted as beam collimators. Each of these sources was preliminary calibrated with their collimator, by using an ORTEC HPGe detector with a diameter of 25 mm, a sensitive thickness of 13 mm and a X–ray entrance window of Beryllium 0.254 mm thick. This preliminary calibration permitted to detect all the γ-ray lines (nuclear, fluorescence lines) with their intensity emitted from the above sources and the presence of very low level X–ray fluorescence from beam collimators.

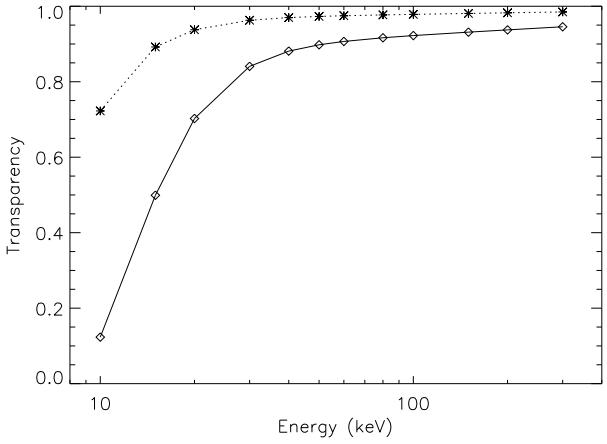

Fig. 3. Transparency of the detection plane window as a function of the photon energy. Dashed line: top shield window transparency. Full line: PHW composite window transparency

3.3. Performance and calibration results

3.3.1. Detector window transparency

The whole transparency of the detection plane windows (phoswich window and top shield window) as a function of the photon energy was determined from the knowledge of the material composition and thickness and it is shown in Fig. 3. Also shown in this figure is the computed transparency of the top shield window alone. The test results were in complete agreement with the values shown. The

absorption coefficients were taken from the EGS4 code data tables (Nelson et al. 1985).

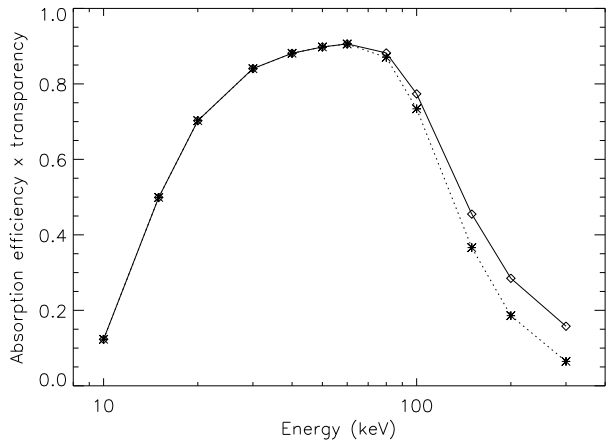

Fig. 4. X–ray absorption efficiency of the NaI(Tl) detection units times the X–ray entrance window transparency. Dashed line: only photoelectric absorption. Full line: total absorption

3.3.2. Detector absorption efficiency

The X–ray absorption efficiency of the NaI(Tl) detectors is defined as $\epsilon(E) = 1 - \mathrm{e}^{-\mu(E)t}$, where $\mu(E)$ is the total absorption coefficient of the crystal and t its thickness. The absorption efficiency times the transparency of the PHW X–ray entrance window is shown in Fig. 4. The thickness t was measured. The PDS detection efficiency is also dependent on the pulse shape thresholds selected, as it will appear from the next section.

3.3.3. Pulse shape discrimination

The pulse shape analysis is of key importance for the experiment performance. The PSA discrimination capability is very satisfactory as can be seen from Fig. 5, that shows a pseudo image (pulse height channel PHA versus PSA channel) of the Hg^{203} radioactive source (nuclear line at 279 keV, plus Tl K-fluorescence lines at ~ 85 and ~ 72 keV). It is apparent the separation of the good events due to NaI(Tl) scintillations (on the left) from CsI(Na) scintillations (on the right) and mixed events (in the middle).

Figure 6 shows the corresponding pseudo image obtained with the Monte Carlo code. It is apparent the similarity of the images apart from an apparent deviation of the measured pulse shape distribution from that obtained with the Monte Carlo code for low PHA channel values that correspond to photon energies in the band from $9 - 15$ keV. This deviation is due to electronic noise. It is also apparent in the simulated pseudo-image the bridge connecting the two hot spots due to 279 keV photons. It is due to Compton interactions of the 279 keV photons that deposit part of their energy in the NaI crystal and part in the CsI crystal.

Figure 7 shows, for detection unit A, the PSA peak centroid and width (2× FWHM) of NaI and CsI crystals as a function of the PHA channel as derived from background measurements. The measurements were obtained at two different temperatures and the separation is very good in both cases. It can be also seen that the centroid position for both crystals is a function of crystal temperature. For the NaI(Tl) we find results consistent with those found in literature (Schweitzer & Ziehl 1983).

Good events are selected by choosing an electronic digital window around "pure" NaI events. Given the dependence of the pulse shape peaks on temperature and, at a lower extent, on energy (see Fig. 7), the window selection can affect the detection efficiency. A too narrow window could decrease the detection efficiency, while a broad window could include many Compton events and thus introduce systematic errors in the spectral reconstruction besides increasing the telescope background level. Actually with our Monte Carlo code we can take into account Compton interactions, single and multiple, and thus obtain an unbiased spectral reconstruction.

A default PSA window (channels 1-70) was chosen to derive the calibration results we report in this paper.

3.3.4. Energy to channel conversion

The nuclear and fluorescence lines emitted from the available radioactive sources, that have an energy below 300 keV, were used to derive the relation between line photon energy and pulse amplitude of the detected line centroids. Figure 8 shows the net Co^{57} spectrum as detected by the phoswich unit A. It is apparent the 14 keV line (on the left) in the detected spectrum. In order to derive the above relation, we fit the source spectra with one or the sum of more Gaussian functions, depending on line separation. For the X–ray fluorescence line blends, we fit to the spectral data the sum of two Gaussian functions due to the K_α and K_β lines, not resolved in our detector. In order to limit the number of free parameters, only the K_α line parameters (line centroid, intensity and FWHM) were left free, while parameters of the other lines in the "blend" were derived as functions of the free parameters, making use of tabulated nuclear spectroscopic data.

The derived relation between line centroid channel and photon energy is shown in Fig. 9 for each of the four phoswich units. The AGC, that was activated during all these tests, provided at 60 keV a gain equalization of the phoswich units within 1.5%. A better equalization (within 0.25%) was obtained during later tests at satellite level. A clear feature of the energy/channel curves is their almost similar behaviour up to 300 keV. This result was obtained thanks to quality control of the NaI(Tl) crystal production and to the fact that all the crystals were cut from the same ingot.

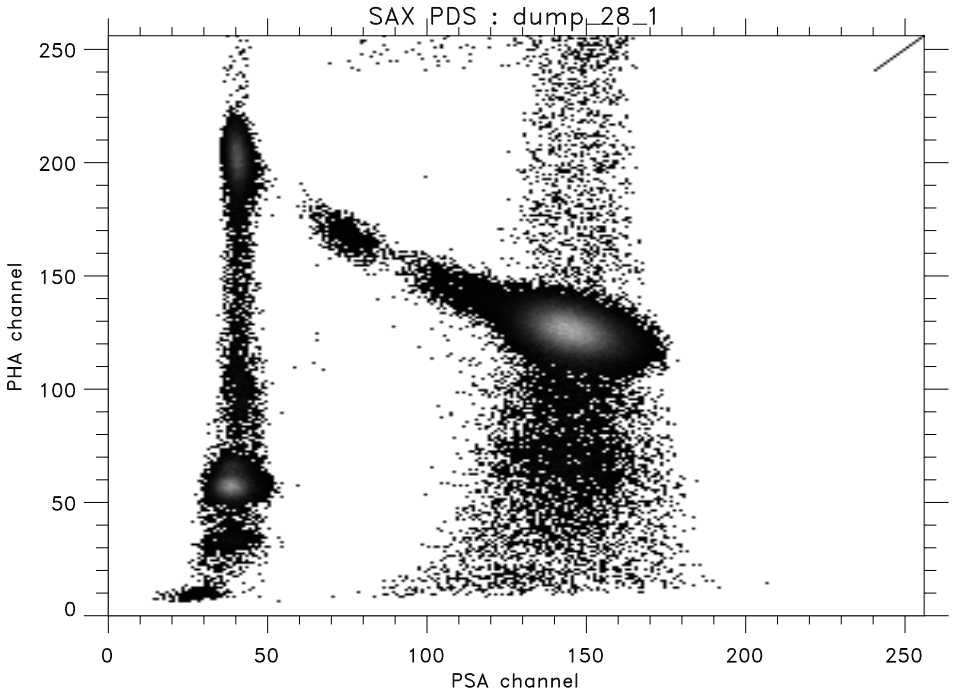

Fig. 5. A pseudo image of the Hg^{203} radioactive source (nuclear line at 279 keV), plus fluorescence X–ray lines at lower energies due to Tl produced in the Hg decay, and to Lead of the source collimator. It is apparent the separation of good events due to NaI(Tl) scintillation (on the left) from events due to CsI(Na) scintillation. It is also apparent a bridge connecting the peaks, corresponding to energy losses in the NaI(Tl) and CsI(Na), respectively. This is due to photons that deposit part of their energy in NaI and part in CsI

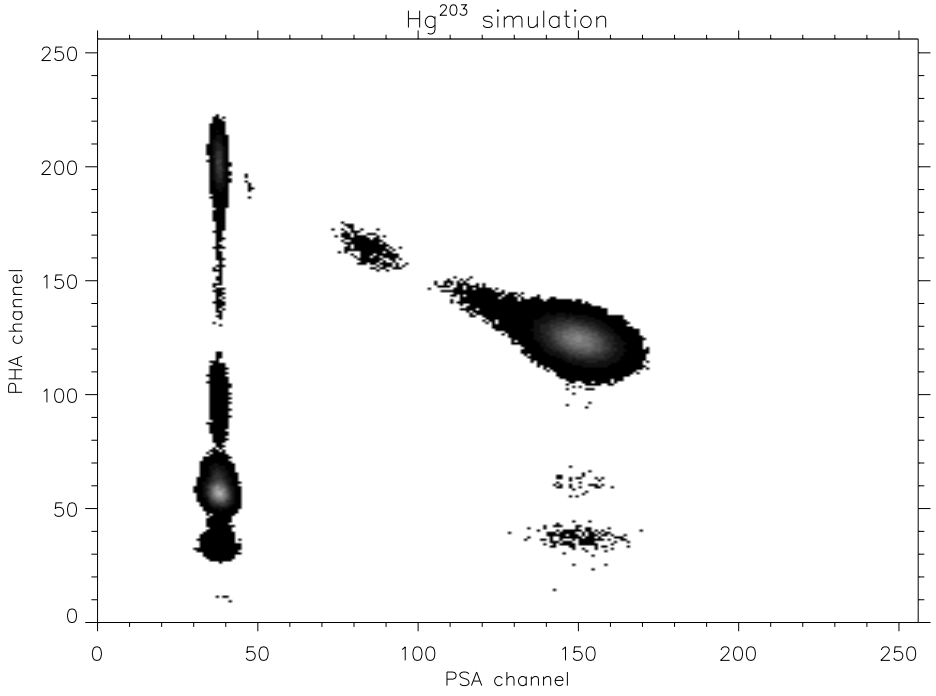

Fig. 6. A pseudo image obtained with a Monte Carlo simulation corresponding to the Hg^{203} radioactive source. It is apparent the similarity with Fig. 5, apart from the lowest energy ($9-15$ keV) photons pulse shape distribution. This deviation is mainly due to electronic noise. Instead is apparent in both the data and simulation images the bridge due to Compton scattering

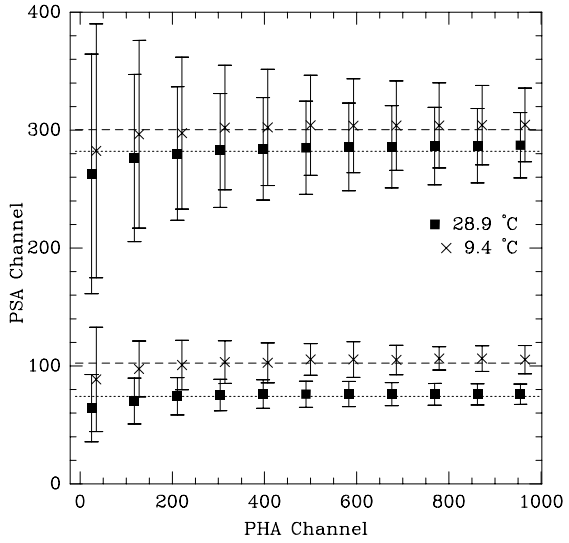

Fig. 7. Position of the pulse shape peaks of NaI and CsI crystals as a function of the pulse height channel as derived from background measurements. Squares (28.9 °C) and crosses (9.4 °C) refer to measurement taken at different temperatures. One error bar is equal to one FWHM of each PSA peak

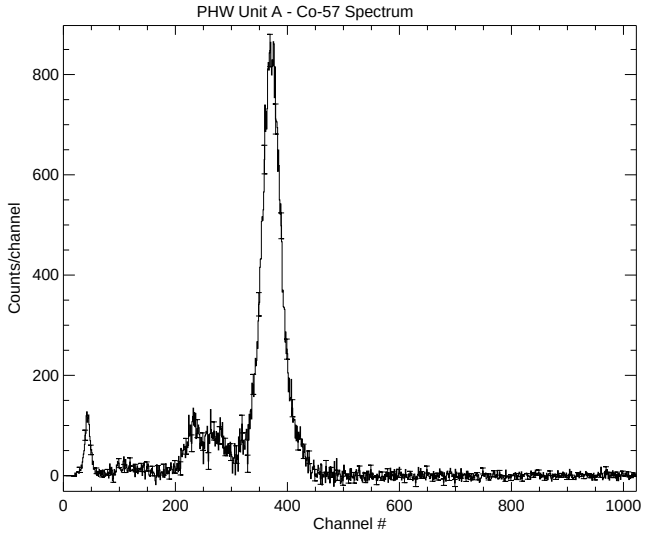

Fig. 8. Background subtracted energy spectrum of the Co^{57} radioactive source used during calibrations as seen by Unit A

The non-linearity curve of each NaI(Tl) crystal as a function of photon energy, normalized to 279 keV Hg^{203} line, is shown in Fig. 10. The curves are in agreement with the expected behaviour of a crystal 3 mm thick (see, e.g., Leo 1987). A detailed investigation of the non–linearity of the NaI(Tl) around the Iodine K-edge (33.170 keV) was not possible using only the available radioactive sources. We plan to perform a thorough investigation of the NaI(Tl) crystal non linearity with the PDS flight spare, whose crystals were cut from the same ingot as the flight model.

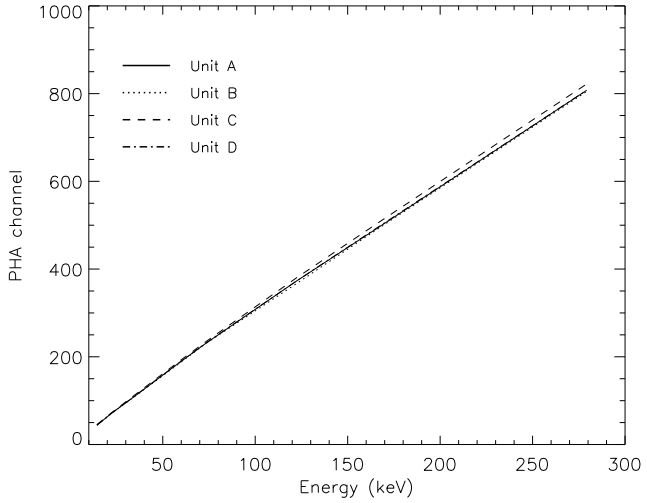

Fig. 9. The derived relation between PHA line centroid channel and photon energy for the four PDS detection units

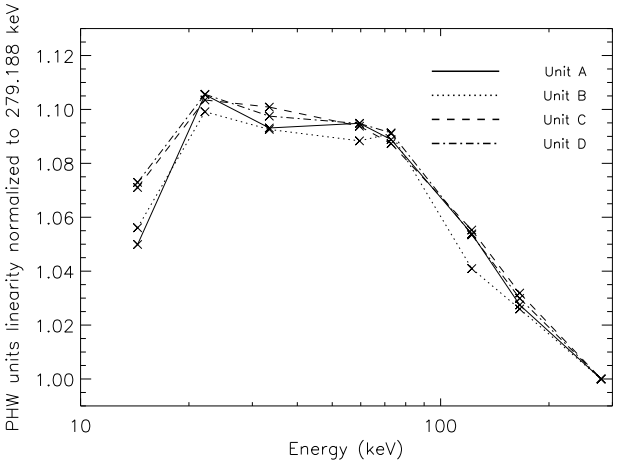

Fig. 10. The non-linearity curve of each NaI(Tl) crystal as a function of photon energy, normalized to the 279 keV Hg^{203} line

3.3.5. Energy resolution

The instrument energy resolution ($R(E) = \Delta E/E$ where ΔE is the FWHM of the Gaussian that fits the detected nuclear line of energy E) was derived by using the same source spectra and results obtained to derive the energy/channel relationship. The behaviour of the energy resolution versus energy of one detection unit is shown in Fig. 11. As can be seen, the data are not fit with a unique power law $R(E) \propto E^{-\alpha}$ with $\alpha = 0.5$ as expected if the scintillator exhibited a linear response up to 300 keV. A broken power law can better fit the data. Actually it is known (Sakai 1987) that the NaI(Tl) scintillators show a deviation from the $E^{-0.5}$ above 100 keV, due to a combined effect of non-linear light output with multiple interactions in the scintillator. In addition we verified (Frontera et al. 1997) that PDS crystal gain is slightly dependent on

photon interaction position across the crystal. This can also affect the energy resolution for high energies where the fractional variation due to Poisson statistics is lower. At 60 keV the average energy resolution of the phoswich units is slightly better than 15%.

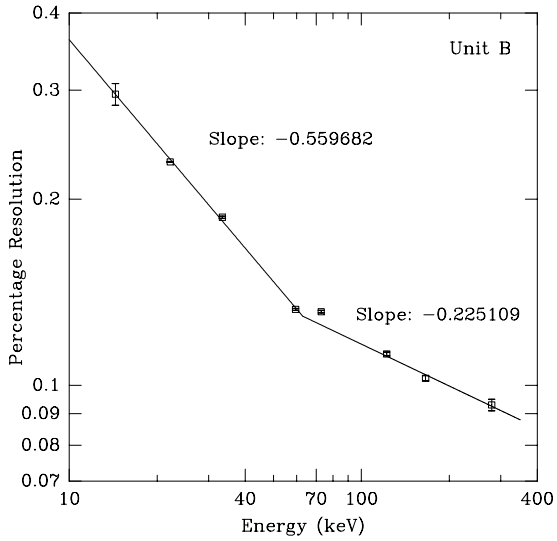

Fig. 11. The energy resolution of the detection unit B as a function of energy. The slopes of two power laws are shown, too. The break occurs at ~ 63 keV

The dependence of the energy resolution on High Voltage (HV) power supply of the phoswich PMT was investigated to determine the interval of HV within which the phoswiches can be operated. Results have already been reported (Frontera et al. 1997). In a range of ± 200 V around the nominal HV (corresponding to 1170−1220 V depending on units) the energy resolution remains constant.

3.3.6. MCS absolute calibration

Figure 12 shows the spectrum acquired from the instrument during a passage of the MCS source across the FOV. By comparing the parameters of the 122 keV line of the MCS source with those obtained when a uniform X–ray beam was incident on the same unit (see Fig. 8), we found that the centroid positions and energy resolutions are consistent each other. The typical time duration of a calibration test is ~ 500 s with live time of the MCS source above each phoswich of 200 s. The count rate due to the 122 keV line was ~ 25 counts/s in March 1996. With this rate the peak centroid can be evaluated with an accuracy of 0.1%.

Due to the decay of the MCS source, the calibration time needed to get the same statistical quality of the data will change with time. After two years the time needed will be 6 times the initial one.

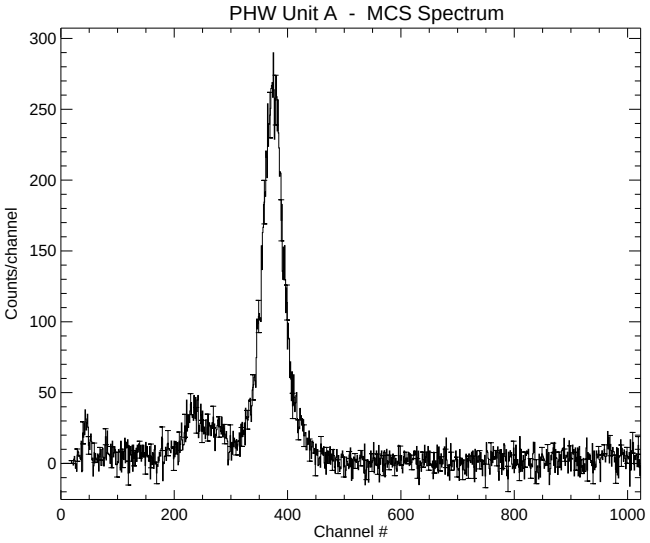

Fig. 12. Background subtracted energy spectrum of the Co^{57} MCS source as seen by Unit A

3.3.7. Effective area

The effective area of the detector units is limited at lower energies by the overall composite window transparency discussed above and at high energies by the NaI(Tl) thickness. It also depends on energy resolution of the detectors and, through it, on incident photon spectrum. The effective area of the entire instrument as a function of energy is shown in Fig. 13, for two different input spectra (power law photon index equal to 1 and 2).

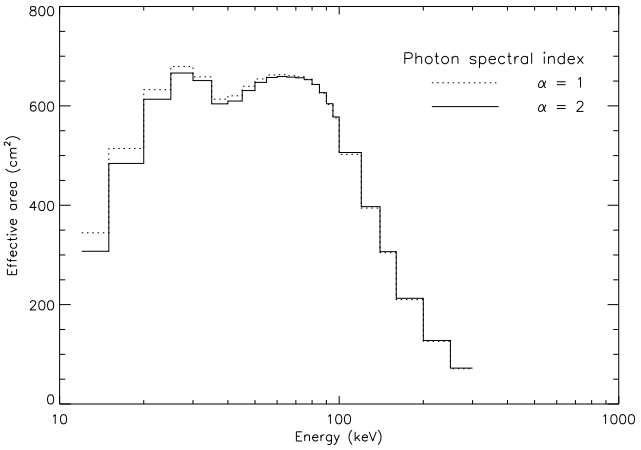

Fig. 13. PDS Effective area as a function of photon energy. Two power law incident photon spectra of the form $E^{-\alpha}$ have been simulated, with photon indices α equal to 1 and 2

3.4. Background counting rate

Great care was taken to minimize the PDS background level. Indeed, the detector materials were selected with low residual radioactivity. The phoswich technique provides an efficient active shielding of the NaI(Tl) detector over 2π solid angle, the lateral AC shielding system provides a rejection of the unwanted photons and charged particles, the AC top shield provides an efficient rejection of charged particles, in particular electrons.

Three background contamination components were identified: non tagged FCS source photons, residual X–ray fluorescence due to rocking collimator materials and contribution from gamma-ray lines of the MCS source. The overall contribution from the first two components gives rise to two main peaks in the background spectrum at 60 keV and 30 keV with an integrated count rate of about 0.3 counts/s per phoswich unit.

The third contamination component derives from photons produced by Compton interactions with the detector materials of weak high energy (> 300 keV) lines of the MCS source. The percentage integrated decay rate due to these lines is 0.18%. For comparison, the percentage decay rate of the 122 keV line is 85%. This contamination component will decay along with the MCS source decay. On the basis of the calibration tests performed in March 1995, this component will contribute with the following rates in September 1996, corresponding to the beginning of the BeppoSAX operative phase: unit A: 0.45 counts/s; unit B: 1.1 counts/s; unit C: 1.1 counts/s; unit D: 0.81 counts/s. As can be seen, different units are affected in different way, depending on their position with respect to the MCS source rest position.

The average background count rate/unit during the system tests at the launch facility (March 1996) was about 2.5 counts/s, corresponding to 4.4 10^{-5} counts/(cm^2 s keV), in the range from 10 to 300 keV. Note that the area in cm^2 refers to the detector geometric area.

No significant background modulation with the rocking collimator offset angle was detected. The upper limit for this modulation, averaged on the entire energy band, is $< 2\%$ (3σ). A detailed calibration of background modulation is foreseen during the scientific verification phase.

4. Data analysis

Concerning the PDS specific software, the following modules will be included in the BeppoSAX data analysis software:

- gain and energy resolution versus energy, using calibration data;
- response matrix calculation (including tabulated data coming from Monte Carlo simulations – see Sect. 3.1);
- background subtraction.

The third module will be tuned following the results of the Scientific Verification phase.

Apart from this analysis software, a dedicated software was developed at ITeSRE, based on a common framework for BeppoSAX S/W (Chiappetti & Morini 1991; Maccarone et al. 1992), for the data acquisition and analysis during ground calibrations (Dal Fiume et al. 1994, 1995). This software allows unpacking of raw data from BeppoSAX telemetry, real time display of selected housekeepings, analysis of calibration data. It can transparently read data both in raw telemetry format and in reformatted FOT format. The data display and analysis section is based on IDL^{TM}. A SQL database based on Ingres^{TM} was also configured to host the results of the analysis of the PDS calibrations during all the pre–operative and operative life of PDS. To this database, we added external facilities to allow easy browsing of the database. The choice of this SQL database was done for the following reasons:

- high reliability due to the high quality of the DB system;
- possibility to embed SQL calls in Fortran and C programs;
- capability to easily design and build GUI interfaces using a native object oriented language.

This software configuration was designed to allow an efficient control of PDS during all its life, with a stable and coherent set of tools, allowing the PDS Scientific Group to answer promptly to the needs of the scientific community in terms of calibrations control, analysis and results. A detailed description of the system will be published elsewhere.

Acknowledgements. The BeppoSAX program and thus the PDS experiment are supported by the Italian Space Agency ASI. Alenia Spazio (Torino), Laben SpA (Vimodrone, Milano), Tecnol (Barberino del Mugello), Bicron (New Bury, U.S.A.) and Officine Galileo (Firenze) with their industrial contracts had a large part in the final PDS design as well as PDS make up. We wish to thank many people who contributed to PDS realization, in particular A. Basili, A. Emanuele, T. Franceschini, G. Landini, E. Morelli, A. Rubini, S. Silvestri and C.M. Zhang for their contribution to the preliminary PDS design and M.N. Cinti who contributed to the analysis of the data from functional tests. Finally warm thanks to R.C. Butler for his continuous skilled and efficient supervision of the PDS final design and realization.

References

Alberghini F., Dal Fiume D., Frontera F., Pizzichini G., 1994, AIP Conf. Proc. 307, 638

Barret D., Vedrenne G., 1994, ApJS 92, 505

Bassani L., Malaguti G., Paciesas W.S., Palumbo G.G.C., Zhang S.N., 1996, A&A (in press)

Bleeker J.A.M., Overtoom J.M., 1979, NIM 167, 505

Butler R.C., Scarsi L., 1990, SPIE 1344, 46

Chiappetti L., Morini M., 1991, BeppoSAX/DAWG Report 15/91

Dal Fiume D., Frontera F., Orlandini M., Trifoglio M., 1994 ASP Conf. Ser. 61, 395

Dal Fiume D., Frontera F., Nicastro L., Orlandini M., Trifoglio M., 1995, ASP Conf. Ser. 77, 387
Frontera F. et al., 1991, Adv. in Space Res. 8, 281
Frontera F., et al., 1992, Il Nuovo Cimento 15C, 867
Frontera F., et al., 1993, IEEE Trans. Nucl. Sci. 40, 899
Frontera F., et al., 1997, Il Nuovo Cimento C (in press)
Kouveliotou C., et al., 1996, Nat 379, 799
Leo W.R., 1987, Techniques for Nuclear and Particle Physics Experiments. Springer-Verlag, Berlin, Heidelberg
Lewin W.H.G., Rutledge R.E., Kommers J.M., van Paradijs J., Kouveliotou C., 1996, ApJ 462, L39
Maccarone M.C., et al., 1992, ASP Conf. Ser. 25, 151
Nelson W.P.R., Hirayana H., Rogers D.W.O., 1985, SLAC-265
Pamini M., Natalucci L., Dal Fiume D., Frontera F., Costa E., Salvati M., 1990, Il Nuovo Cimento 13C, 337
Piro L., Scarsi L., Butler R.C., 1995, SPIE 2517, 169
Sakai E., 1987, IEEE Trans. Nucl. Sci. 34, 418
Scarsi L., 1993, A&AS 97, 371
Schweitzer J.S., Ziehl H., 1983, IEEE Trans. Nucl. Sci. 30, 380
Zhang S.N., et al., 1996, A&A (in press)